Investigation into the influence of threshold forces and vibrations in diamond roll plunge dressing of grinding wheels

By

Douglas J. Geiger

A Thesis

Submitted to the Faculty

of the

WORCESTER POLYTECHNIC INSTITUTE

in partial fulfillment of the requirements for the

Degree of Master of Science

In

Manufacturing Engineering

May 2005

APPROVED:

Prof. Christopher A. Brown, Major Advisor

Dr. Robert S. Hahn

Dr. John Kummailil

Abstract

This work investigates threshold forces and vibrations in diamond roll plunge dressing of vitreous bonded aluminum oxide grinding wheels. Threshold forces in dressing are not currently considered in the control of the dress cycles of grinding wheels in manufacturing. These threshold forces, however, can lead to size, taper, and out of round errors on the grinding wheel, which are then imparted onto the workpiece. Particularly in internal grinding, and other setups with lower spindle stiffnesses, any threshold force in dressing will cause deflection of the spindle before removing abrasive, which will lead to the grinding wheel being out of size. Hall-effect sensors on the grinding wheel spindle are used to determine the normal force, and a linear encoder on the dressing roll cross-slide is used to determine the abrasive removal rate. The abrasive removal rate is plotted against the normal force for a number of feedrates, and two distinct slopes were observed, with two different threshold forces. In addition, an acoustic emission system is compared to the hall-effect force sensor to study the correlation of the two sensors.

Forward

This thesis is based on a paper submitted to the Journal, titled **Measurement and Analysis of Forces in Diamond Roll Dressing**, by John Kummailil, Douglas Geiger, Robert Hahn, and Christopher Brown, which was submitted to the Journal of Manufacturing Processes in March, 2005

Acknowledgements

Thanks to Saint-Gobain for their commitment to manufacturing education in New England through the Saint-Gobain Professorship, graduate fellowships, equipment improvement grants and supplies. In particular, we would like to thank John Webster and David Graham, both of Saint-Gobain, for their advice and assistance in providing us with grinding wheels.

Thanks to Fabio Ferraz and Prof. João Fernando Gomes de Oliveira from Universidade de São Paulo for supplying the acoustic emissions detection equipment and expertise.

I would like to thank Robert Hahn, John Kummailil, and Christopher Brown.

1 Introduction

1.1 Objective

The objective of this work is to determine if threshold forces exist in diamond roll plunge dressing of grinding wheels, and to investigate vibrations during the dressing cycle.

1.2 Rationale

1.2.1 Grinding/Dressing Operations

Quantifying threshold force phenomena is essential to optimizing grinding wheel sharpness, controlling the dimensions, and controlling chatter, all of which can impact ground part quality and alter yield. In some processes, grinding wheels are periodically dressed by plunge feeding the wheel into a diamond roll. It is commonly assumed that the roll cuts the wheel upon contact and produces a true-running, cylindrical, dressed wheel. However, if a threshold force does exist, the amount of material removed will be lower than it would be if it did not. This could affect the dimensions of parts the wheel subsequently grinds.

This concept can be illustrated by assuming the existence of a threshold force, F_{th}. A conservative dressing operation would compensate for wear by indexing the dressing roll by an amount $(h + \Delta h)$ with respect to the previous dressing position for the grinding wheel, where h is the expected wheel wear since the previous dressing operation, and Δh is the amount of overcompensation. Overcompensation is usually done to sharpen the grinding wheel and to remove any chatter on the wheel surface. The normal dress force generated during the dressing, F_n, can be represented as $F_n = K_{sys}\Delta h$, where K_{sys} represents the stiffness of the machine elements supporting the dressing roll relative to the grinding wheel.

If a threshold forces exists, and if $F_n < F_{th}$, the wheels would rub together without removing material, causing the grinding wheel diameter to be off by Δh. If the next

n dressing operations similarly fail to remove material, the grinding wheel diameter would be off by $n \times \Delta h$, until the grinding wheel is large enough compared to its excepted size so that the threshold force is exceeded $(F_n > F_{th})$, and the dressing roll removes material from the grinding wheel. In any event, if a threshold force exists, the dimensional accuracy in the grinding wheel and the parts it subsequently produces will be reduced.

Aside from influencing the dimensions of the parts produced, the rubbing that occurs when the threshold force is not exceeded would most likely reduce the sharpness the grinding wheel and thereby influence the surface of the work piece. Therefore, threshold forces in diamond roll dressing could lead to erratic grinding cycles and can cause parts to be rejected.

2 Equipment and Data Collection

2.1 Experimental Setup

2.1.1 Force Adaptive Grinding Machine

A Hahn Force Adaptive Grinder (Hahn Engineering Inc, Auburn, MA) was used in this study. Figure 2.1 shows the schematic of the Hahn force-adaptive grinding machine. The grinding wheel is mounted on a shaft driven by a 5 horsepower, 3600 rpm AC motor (Pope, Haverhill, MA), controlled by an open-loop motor controller. The dressing roll is mounted on a shaft, which is rotated by a permanent magnet DC servomotor (Powertron, Charlotte, NC).

The servos are controlled by a Delta Tau PMAC controller, which is in turn controlled by a PC-based computer with customized software developed by Hahn Engineering, Inc.

2.1.2 Sensors

The grinding wheel shaft is fitted with two opposing Kaman Hall-effect displacement sensors (Kaman Measuring Systems, Colorado Springs, CO). The sensors are mounted parallel to the direction of shaft deflection to detect the normal component of the dress

force. A force acting on the shaft inline with the two sensors, displaces the shaft relative to the sensors and causes the sensors to produce a voltage that is proportional to the force acting on the shaft.

The crosshead servomotor is fitted with a linear encoder that outputs voltage pulses as the crosshead moves. The number of pulses indicates the crosshead displacement.

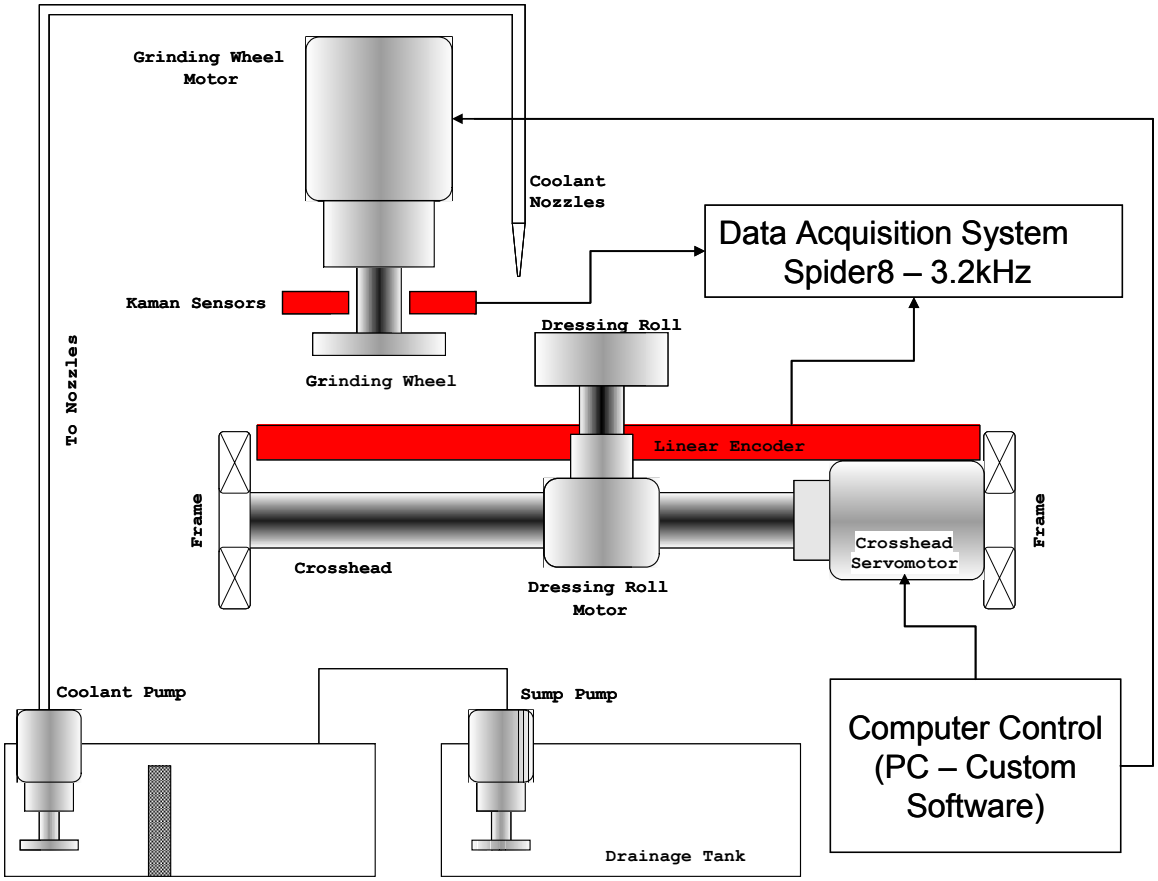

Figure 2.1: Schematic of the Hahn Force-adaptive Grinding Machine

2.1.3 Data Acquisition

The voltage signal is captured by a Spider 8 16-bit data acquisition system (Hottinger Baldwin Messtechnik GmbH) at 3.2 kHz. The channels are synchronized by a master clock within the Spider 8 so acquisition occurs simultaneously.

2.1.4 Grinding Wheel Shaft Properties

The stiffness of the grinding wheel shaft was measured relative to the housing by applying a load parallel to the crosshead motion and measuring the corresponding displacement using a Microtrol electronic indicator (L. S. Starret Co., Athol, MA). The load was aligned with the normal component of the dress force. The Kaman sensor output was recorded at each load by the Spider 8 to obtain the voltage-force conversion factor.

2.2 Filter Development

The Kaman sensors are susceptible to noise from a variety of sources, necessitating the use of filters. Sources of noise include variations in shaft diameter and ambient electrical noise. These noise frequency components must be characterized, to design filters that do not significantly attenuate force data. If the shaft is not perfectly cylindrical, its position relative to the sensor will vary as the shaft rotates, causing voltage excursions. Precession about the axis of rotation also has the same effect. The following sections discuss methods used to identify noise components, so effective filters can be designed.

2.2.1 Noise Frequencies

To characterize the noise frequencies present in the environment as well as the grinding machine itself, a series of recordings was made by sequentially powering up one component at a time to isolate its contribution to the overall noise in the signal.

Table 1 shows the recordings taken while sequentially powering up components of the machine. A baseline noise signal was obtained by recording the force sensor signal at 3.2 kHz with all machine components turned off. Power spectra were generated using the Signal Processing Toolkit of MATLAB and the peak locations were used to design filters.

Table 1: Noise Frequency Tests

Mnemonic	Grinding Wheel Motor	Dressing Roll Motor	Coolant Pump	Sump Pump
Ambient Noise				
Pumps				•
Dressing Roll Motor		•	•	•
Grinding Wheel Motor	•		•	•
Both Motors + Pumps	•	•	•	•

Spectral analysis of the force signals (not discussed in detail in this paper) showed frequencies around 420 Hz growing in magnitude as dressing progressed. This has been identified as the systems' natural frequency in its unloaded state.

2.2.1.1 Force Signal Conditioning

The following procedure was used to convert the measured voltage signal to the instantaneous normalized, normal force $F_n'(t)$:

- A baseline voltage was calculated by averaging the first 3200 points, during which the wheel and roll were spinning but not in contact.
- The baseline voltage was subtracted from the filtered signal.
- The voltage signal was smoothed using one of several low-pass filters.
- A left-shift was applied to correct for the phase shift of the filter, if appropriate.
- The voltage-force conversion was performed using $F_n(t) = K_{vf} \times V(t)$, where $K_{vf} = 713.04\left(N/Volt\right)$.
- The normalized, normal force $F_n'(t)$ was obtained by dividing every point in the signal by the width of the wheel.

Concerns over the effect of filtering on threshold forces were addressed by running the data through a variety of filters. Widely different parameters were used to design these filters. Two types of filters were used: moving average filters and finite impulse response (FIR) filters. Moving average filters were characterized by the size of their windows – the number of data points averaged. Smaller windows average fewer points and therefore smooth the data less. Larger windows smooth the data more, but attenuate sharp changes in the data. A window width of one is the equivalent of not filtering. A window width of 3200 corresponds to 1 second of data, given the data acquisition rate used in this study. The FIR filters were standard equiripple filters (Proakis and Manolakis, 1996) in which the only parameter changed was the cut-off frequency.

2.2.2 Encoder Signal Conditioning

Figure 2.2 shows the movement of the crosshead through the one dressing test. The crosshead servomotor brings the diamond roll and the wheel 50 μm away from each other before the test begins.

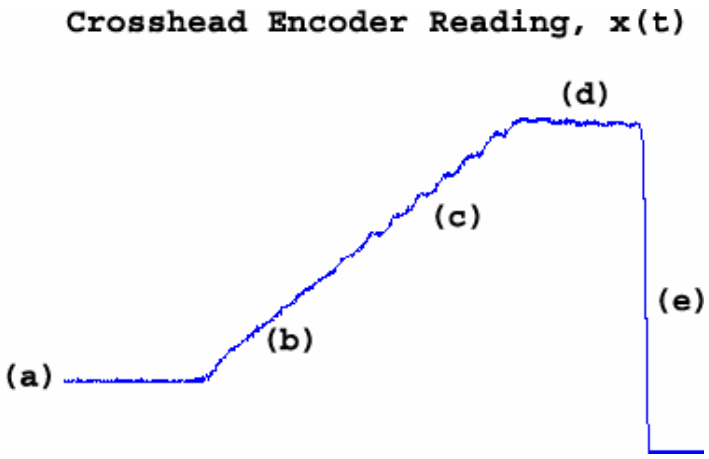

Figure 2.2: Motion of the crosshead: (a) wheel and roll are 50 μm apart. (b) the crosshead starts moving at commanded velocity. (c) contact is made. (d) crosshead motion stops. (e) crosshead returns to home position.

Referring to Figure 2.2, data acquisition starts on the encoder signal, (a), before the stages start moving. The crosshead moves at the selected feed rate, (b), across the 50 μm separating the grinding wheel and the dressing roll (according to the encoder – the program records the encoder reading from the previous test, which establishes the location of contact, provided the threshold force was exceeded during that test). This brings the dressing roll and the grinding wheel into contact at the desired feed rate. Once contact is made, (c), the crosshead moves 75 μm further (d), then stops, and reverses direction, (e), moving the grinding wheel and the dressing roll apart at high speed. Spark-out occurs in the time the crosshead is stationary, though it may not proceed to completion before contact is broken. Note the appearance of a cyclic component after contact, indicating that the crosshead is moving at a non-constant velocity, therefore removing variable amounts of material.

The normalized material removal rate, $Q'(t)$, was calculated from the encoder readings as follows:

- The instantaneous crosshead feed rate was calculated using $u_x(t) = \frac{dx}{dt}$, using consecutive encoder readings to calculate dx.
- A 3200-point moving average was applied after all negative values were set to zero. (Negative values can occur at high data acquisition rates when the encoder flickers between consecutive readings. Since data acquisition is at a much higher rate than the encoder values typically change, the encoder may be straddling adjacent readings when polled. In this case, the encoder randomly returns one or the other of the readings it is straddling. Inevitably, this sometimes leads to negative values when velocity is calculated using the formula above, which causes the apparent reversal of direction of stages).
- The normalized material removal rate was calculated from the corrected displacement using $Q'(t) = \pi \times D_{avg} \times u_x(t)$, where D_{avg} was the average diameter through the whole series of tests.

2.2.3 Definition of Analysis Windows using $F_n(t)$ and $Q(t)$

Some residual noise survived in the filtered signal, making it difficult to precisely define the point of contact. Therefore, the analysis window (defined below) was restricted to a region where contact was well established. This ensured that the data being processed was acquired when the roll and the wheel were moving together in what we define to be unambiguously in contact, which in reality is may be intermittent, at the commanded feed rate

The moment when the force reached 75% of the maximum was used to determine the start of defined contact between the wheel and the roll. End of contact is difficult to establish from the force signal because spark-out commences while the stages reverse direction. Because of spark-out, there is no abrupt drop in forces that could be obviously used to define an unambiguous end of contact. The last $Q'(t)$ value to exceed 80% of the maximum was used. The middle $5/7$ of the time between the defined start and end of contact was used in the generation of the threshold force plots. The assumption is that data in the middle $5/7$ must have been recorded while the wheels were in at least strong intermittent, contact and moving together at a near constant velocity. Note, the calculated Abrasive Removal Rate shows a non-zero value before contact has begun, and thus is ignored until the start of the analysis window.

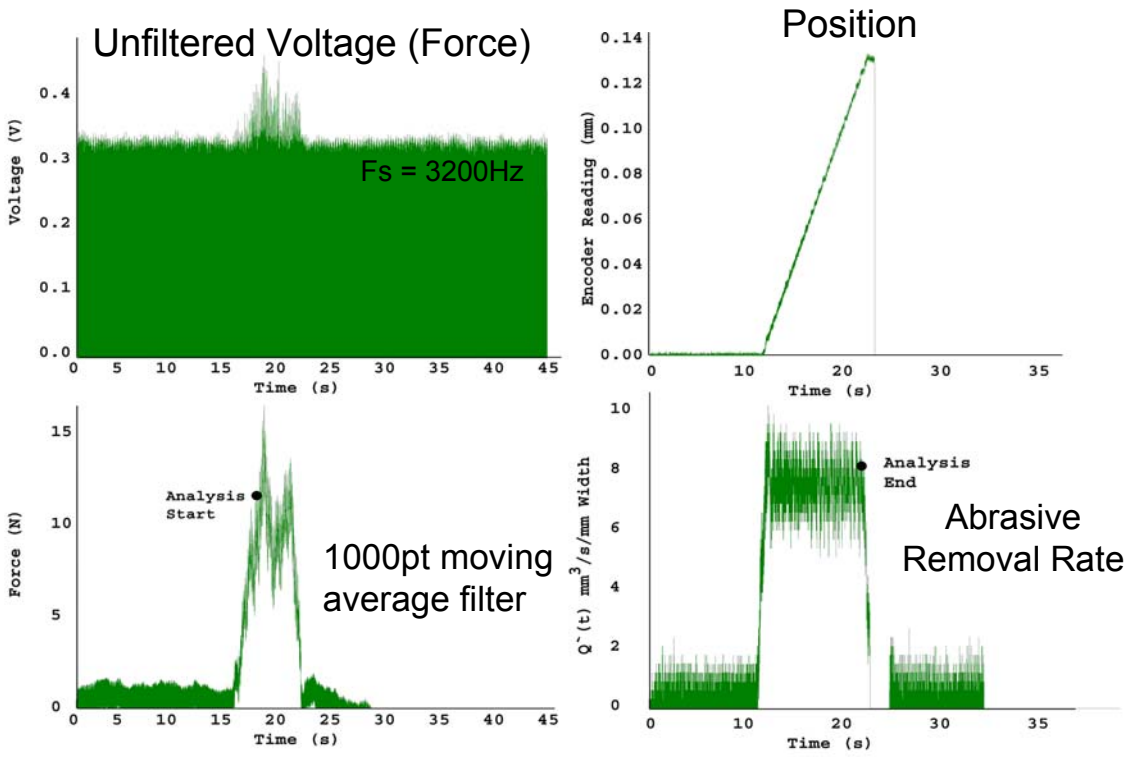

Figure 2.3: Raw and filtered voltages, and encoder data

2.3 Experimental Procedure

The plunge dressing tests were run on a grinding wheel (3SG80-MVS, 7x1/2x1-1/4, Saint-Gobain, Worcester, MA) rated at 3600 rpm. The wheel was 177.8 mm in diameter, 12.7 mm in width and had an inner hole with a radius of 31.75 mm for mounting on the shaft. The wheel was dressed to establish the location of its edge before experiments began. The diameter was 174.73 mm as measured by a Starrett vernier caliper (12 inch span).

In industry, dressing is typically used to remove fixed amounts of material and is usually displacement controlled. This series of experiments was designed to parallel industry practices and 75 µm of material was to be removed in each operation. Since the dressing

operations were programmed to remove equal amounts of material at different feed rates, cycle times were dependent on the feed rates used.

A series of 54 plunge-dressing tests were performed at 18 feed rates from 0.25 mm/minute to 9 mm/minute. A three-minute interval was allowed between successive tests to let the system approach thermal equilibrium.

The crosshead motion during every test was as follows:

- The crosshead servomotor moved the dressing roll 50 μm away from the grinding wheel and stopped.
- Data acquisition began on the Kaman sensor and the crosshead servomotor encoder outputs.
- The crosshead servomotor received the feed rate signal and began moving.
- If the dress force exceeded the unknown threshold force, 75 μm was dressed from the grinding wheel, if not, an unknown amount of material was removed.
- The crosshead servomotor received the return command and reversed direction.
- The crosshead returned to the home position at a rapid feed rate.

The force sensor output and encoder position were recorded simultaneously at 3.2 kHz. All other settings on the equipment were maintained constant. The diameter of the wheel was measured using the vernier calipers after each series of three tests.

3 Results

3.1 Abrasive removal rate vs. Normal Force

From the position data, abrasive removal rate is calculated by dx/dt, where x is the current position of the cross-slide. The normalized force per unit wheel width is calculated based on the wheel width of 12.7 mm.

3.1.1 Threshold Plots

3.1.1.1 Raw Data

Figure 3.1 shows Q'(t), the normalized material removal rate, plotted on the ordinate, with F'(t) the normalized normal force, is plotted on the abscissa, for several different feed rates. Only the middle five sevenths between the start and end of contact is used in the plot. Each color on the graph represents one feed rate. Filled circles represent the average value of one trial at one feed rate. Similar graphs were made by processing the signals using different filters.

Figure 3.1 shows that force excursions increase with feed rates. The scatter in force measurements within a test span approximately 2.5 N and may be due to mechanical vibrations, which increase with feed rate. The averaged force excursions for each test are plotted as black dots in Fig. 3. The averaged force excursions between tests run under the same feed rates appear to lay relatively close together – the largest range is only about 0.75 N at a feed rate of 8 mm/min.

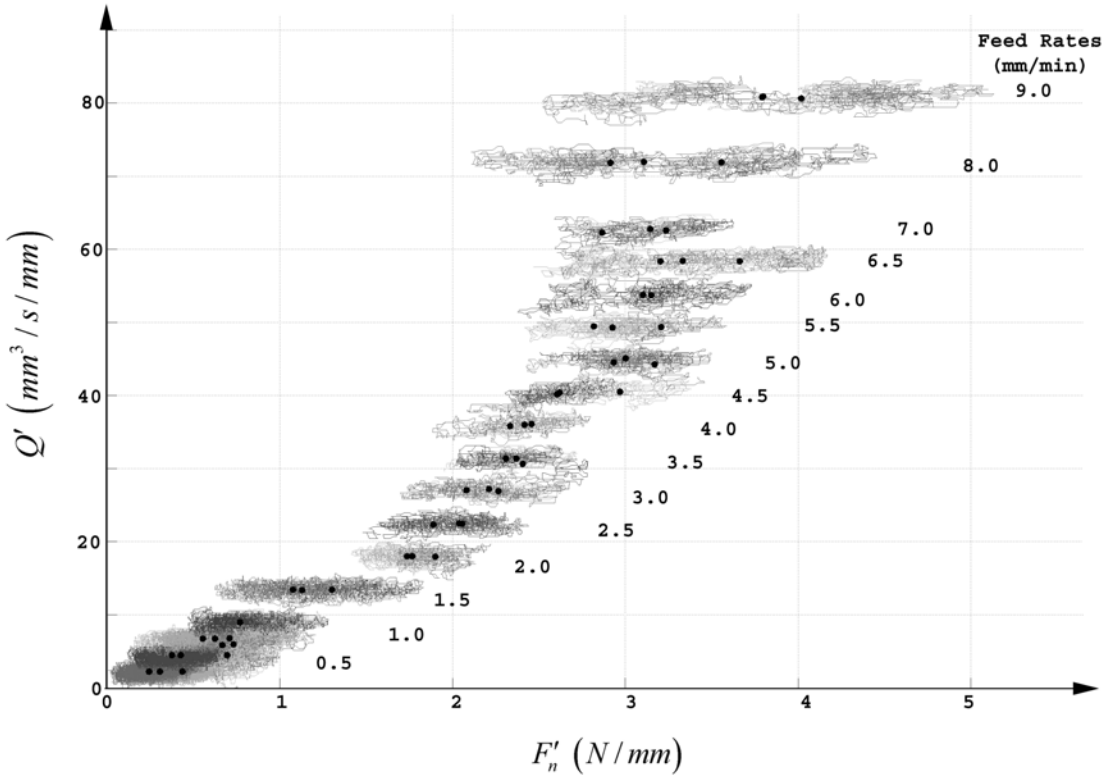

Figure 3.1 Threshold Plot for MVS wheel. Normalized forces are plotted against the normalized material removal rates as functions of time. The feed rates are noted on the figure.

1. At any feed rate the variation in material removal rates encompass about 4 mm^3/sec/mm. The scatter could be a result of servomotors adjusting the cross head feed rate as they strive to maintain the commanded value.

3.1.1.2 Averaged Data

When only the mean values at each feed rate are plotted, Figure 3.2, the threshold charts look similar to those for force-controlled grinding of "difficult-to-grind materials" (1971), which show a distinct region of low material removal rate below a threshold force. Consistent with expectations, material removal rates are higher and forces are lower for dressing than for grinding.

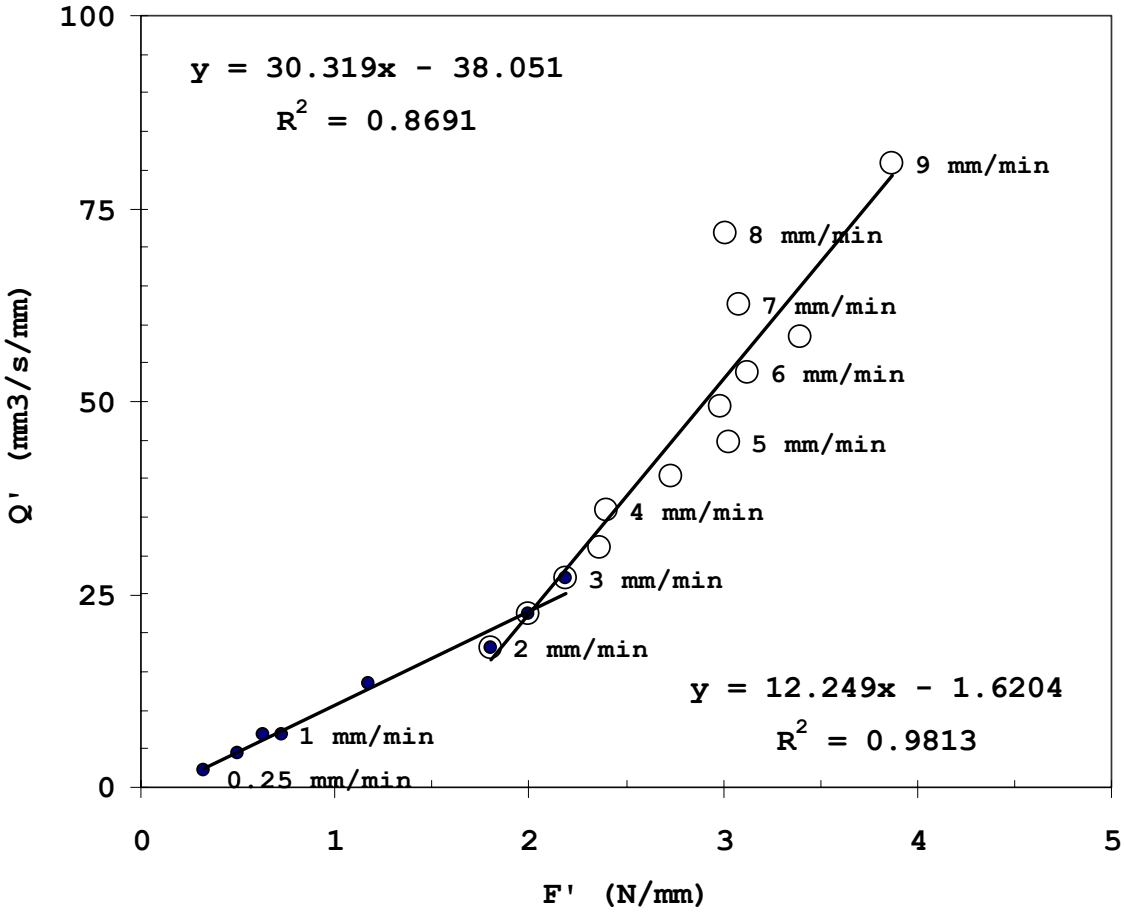

Figure 3.2 Threshold plot with 1000 point moving average filter. The averages are plotted to show the two slopes.

Malkin (1989), quoting the Lindsay and Hahn (1971) study, suggests the wheel sharpness might be one reason for the two slopes, since sharpness is dependent on both material removal rate and dressing time. Other plausible reasons for the two slopes might be the intermittent contact due to roll run-out, or wheel loading.

It was noted that at high feed rates, threshold forces appear independent of the window size of the moving average filter, provided the window size is below 2000 data points (0.6 seconds of data). This is expected, as the dressing time at the highest feed rate of 9000 μm/minute is 0.5 seconds (1600 data points). Any further increase in window size would average the build up and decline of forces, reducing the value reported. The high

feed rate signals would be reduced more because dressing occurs for shorter times, which would reduce the slope of the line and lower the threshold. The same reasoning may explain why thresholds for the 12 Hz cut-off FIR filter and the 1000-point moving average filter are so close.

3.1.2 Influence of Filtering

Table 2 shows the different filter types the parameters that were varied and effect of various frequencies on the threshold forces. At high feed rates, threshold forces appear independent of the window size of the moving average filter, provided the window size is below 2000 data points (0.6 seconds of data). At low feed rates, the threshold forces also appear to be independent of the filter used, provided the window size is less than the minimum dressing time of 0.5 seconds. Moving average filters with window size of 1 and 10,000 are shown to illustrate the unfiltered and over-filtered extremes and are not included in the calculation of the average normalized threshold force, *F'th*,

Table 2 Effect of filtering on Threshold Forces

Filter Type	Window Size (points) or Filter Order	Seconds of Data* (seconds)	Threshold Force (N)	
			Low Feed Rates	High Feed Rates
Moving Average	1	0.0003	0.14	0.70
Moving Average	10,000	3.1	0.28	0.02
Moving Average	100	0.03	0.08	1.12
Moving Average	500	0.16	0.11	1.18
Moving Average	1,000	0.3	0.12	1.16
Moving Average	2,000	0.6	0.15	1.08
FIR, 3 Hz cut-off	2,756	N/A	0.14	1.28
FIR, 5 Hz cut-off	1,378	N/A	0.15	0.82
FIR, 12 Hz cut-off	1,378	N/A	0.09	1.14
Average Normalized Threshold Force, *F'th* (N/mm)			**0.12**	**1.11**

* Values have been rounded for clarity. Window Size applies to moving average filters; Filter Order applies to FIR filters.

3.2 Force vs. Time – Peak/Steady-State

3.2.1 Characteristic Force-Time Curve

3.2.1.1 Typical Grinding Curve

Typical grinding force-time curves with a constant in-feed (as opposed to constant-force) show a logarithmic growth to a steady-state force Figure 3.3. This is due to the initial deflection of the system (King & Hahn, 1986). As the force exceeds the threshold required to remove material, the force begins to level off and reaches a steady state.

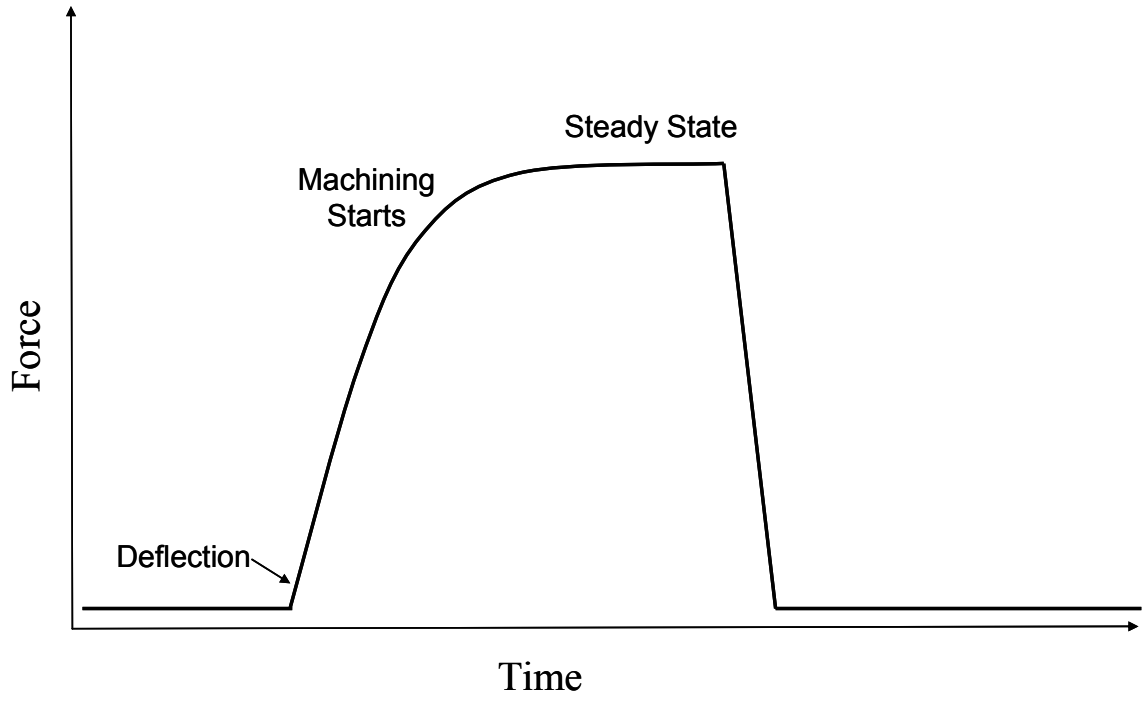

Figure 3.3: Typical Grinding Force-Time Curve (Constant Feedrate)

3.2.1.2 Dressing Curve

In the dressing experiments, a characteristic force-time curve was observed (Figure 3.4), with an initial build up with a constant slope (due to deflection), a peak force, which is feed rate dependant, and then a drop to steady state. This is a similar curve as is observed with dull CBN wheels, that self-sharpen during the grinding cycle (Malkin, 1989, pp.132-133). The initial slope is linear, indicating that no abrasive removal occurs during that period. When some peak force is reached, abrasive removal begins, and the force drops to a steady-state force, with constant abrasive removal until spark out.

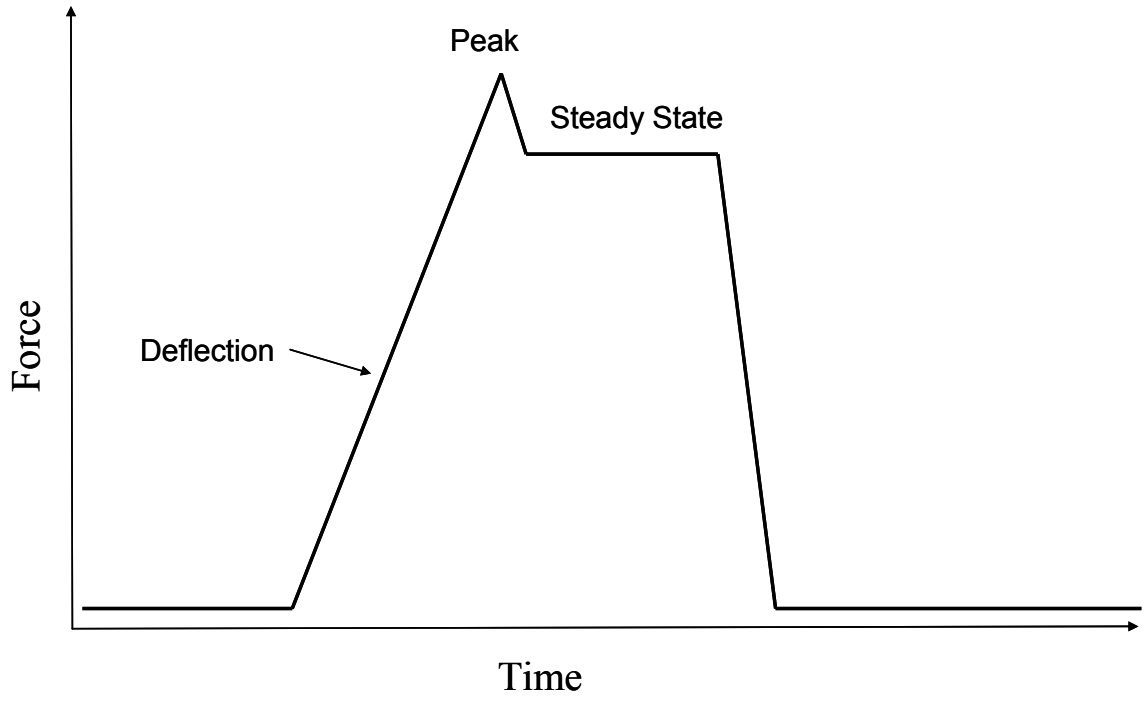

Figure 3.4: Typical Dressing Force-Time Curve

3.2.2 System Stiffness

3.2.2.1 Measured System Stiffness

The system stiffness was obtained using several methods: by measuring the stiffness of individual components, and calculating the total system as a system of springs in series

$$\frac{1}{K_{sys}} = \frac{1}{K_1} + \frac{1}{K_2} + \frac{1}{K_3}$$

Where K_{sys} is the system stiffness, and K_1, K_2, and K_3 are the stiffnesses of the individual components.

3.2.2.1.1 Individual Components

Applying known loads to the Pope wheel head, and the Whitnon head (thus capturing the grinding wheel spindle stiffness, the dressing roll stiffness, and the static stiffness of the crosshead ball screw with the servos off), and measuring the deflection with an indicator. This measurement gave a system stiffness of 1500 N/mm. It is important to note this measurement does not take into account the wheel/roll interface.

3.2.2.1.2 System in Contact (Laser/Mirror)

The dressing roll is brought into contact with the grinding wheel by hand turning the ball screw, with the system powered off. A load is then applied to the ball screw, and the rotation of the screw is monitored using a mirror attached tangential to the screw with a laser illuminating a spot in the center of the mirror, and the location of the laser dot recorded on a paper on the wall opposite the machine.
This measurement gave a system stiffness of 800 N/mm.

3.2.2.2 Calculated System Stiffness

3.2.2.2.1 $\frac{dF}{dt} = K \cdot v_f$

Assuming no material removal occurs in the initial slope of the force-time curve, then the equation: $\frac{dF}{dt} = K \cdot v_f$ holds. Plotting the initial slope versus feedrate gives the plot shown below (Figure 3.5). There is a clear linear progression of initial force slope versus feedrate.

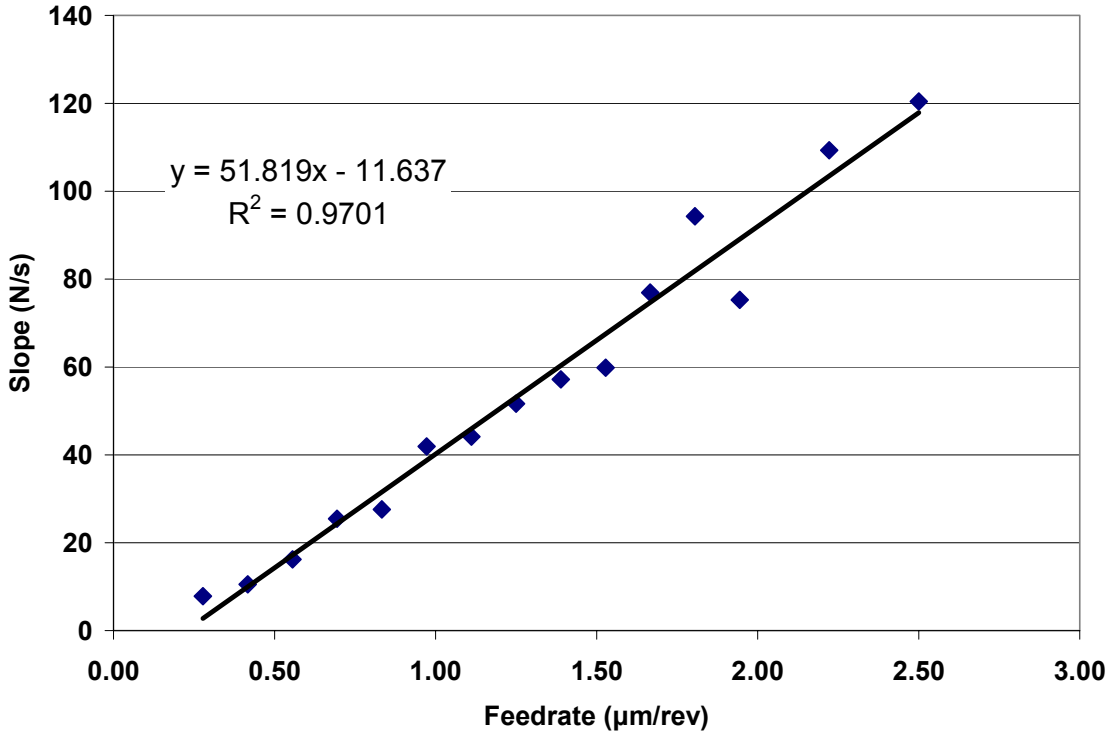

Figure 3.5: Initial Force Slope vs. Feedrate

Using those slopes, solving the equation dF/dt = K*v_f for K, gives the following graph of stiffness versus feedrate (Figure 3.6). There is a clear rise in stiffness with feedrate, indicating a non-linear component to the system. If the stiffness is again taken to be a system of springs in series, then the non-linear wheel/roll stiffness (K_a) can be backed out:

$$\frac{1}{K_{sys}} = \frac{1}{K_s} + \frac{1}{K_w} + \frac{1}{K_b} + \frac{1}{K_a}$$

$$K_a = \frac{1}{\frac{1}{K_{sys}} - \frac{1}{K_s} - \frac{1}{K_w} - \frac{1}{K_b}}$$

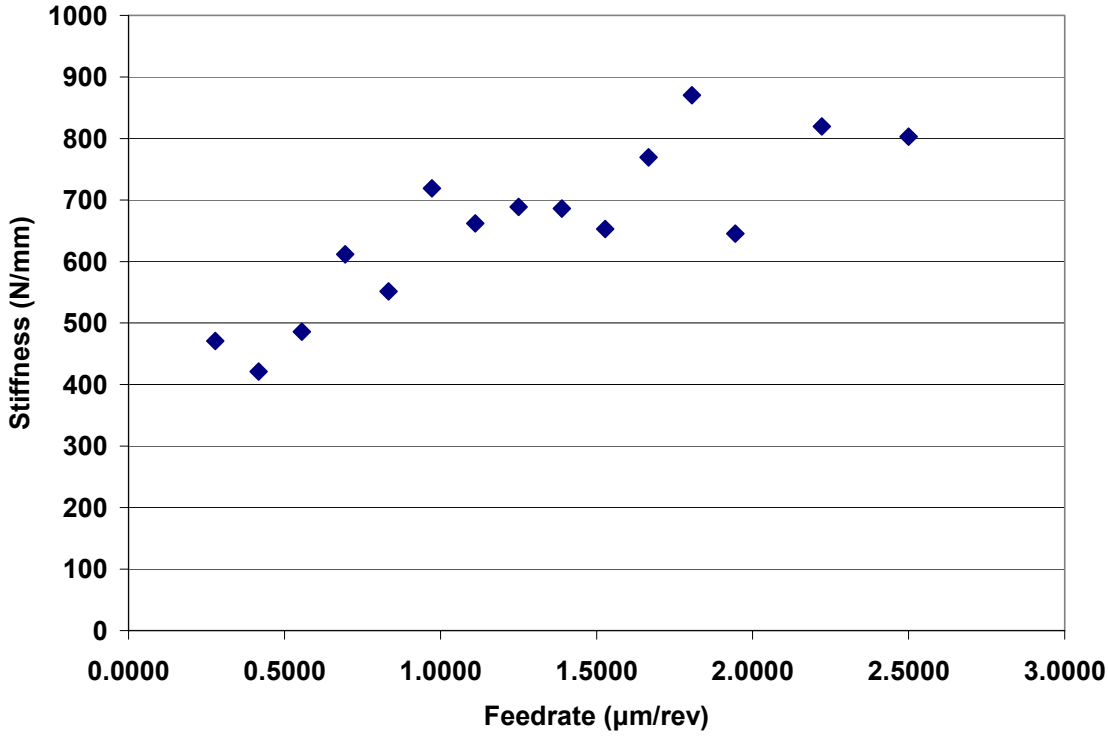

Figure 3.6: Calculated Stiffness vs. Feedrate

Where K_s is the grinding wheel spindle stiffness (4604 N/mm), K_w is the dressing roll spindle stiffness (9667 N/mm), and K_b is the ball-screw stiffness (2888 N/mm). The resulting calculated K_a is shown in Figure 3.7.

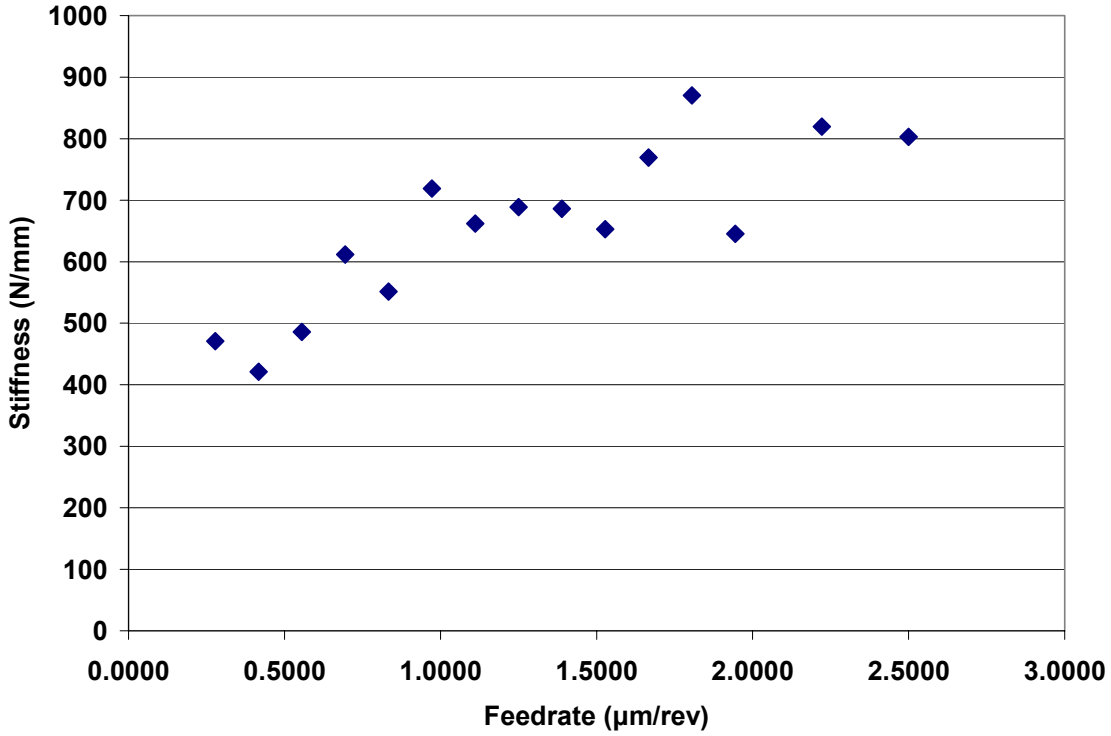

Figure 3.7: Calculated Wheel/Roll Interface Stiffness

3.2.3 Vibrations and Acoustic Emissions

3.2.3.1 Spectrogram

The spectrogram is a useful tool for performing time-frequency analysis. Figure 3.8 shows the frequency components in time present in the raw force sensor signal. The x axis shows the time the component is present, the y axis shows the frequency of the component, and the color represents the magnitude of the frequency component at that particular time. In this case red represents a high magnitude, and blue represents low magnitude. Two vertical lines represent the start of contact in the dress cycle, and the peak force. Of particular interest, is the area near 370 Hz, that appears just before the peak force occurs, and remains until the end of the dress cycle (17s – 23s). The

uncoupled grinding wheel spindle has a natural (ringing) frequency near 420 Hz, so this component near 370 Hz is believed to be the natural frequency of the system in contact. The high magnitude of this frequency suggests the presence of wheel-regenerative chatter during the dressing cycle.

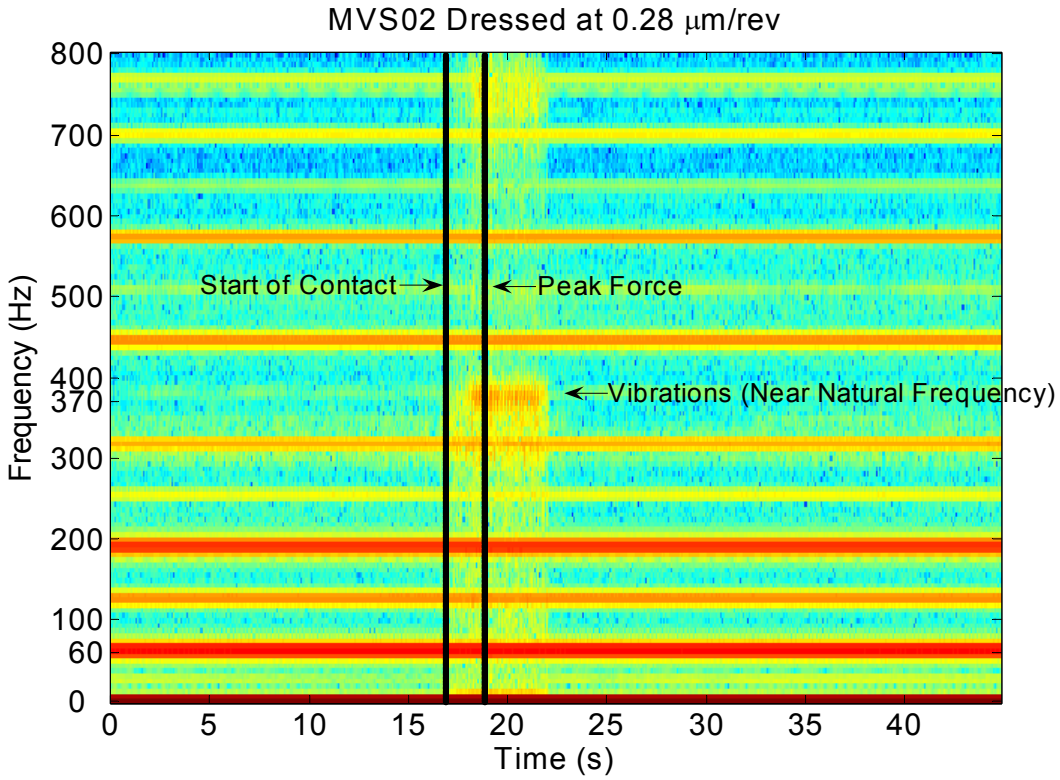

Figure 3.8: Spectrogram from raw force sensor data

3.2.3.2 Acoustic emissions sensor

An acoustic emissions sensor was fitted to the grinding machine near the dressing roll. Two sensor attachment points were used; the first was magnetically mounted to the base of the dressing roll spindle. This setup did not have a desirable signal to noise ratio (SNR), and a second sensor, which allow coolant to flow through it. This coolant could then be directed to spray onto the wheel/roll contact area, and acoustic emissions would flow backwards through the coolant, to the sensor. The data shown below (Figure 3.9) comes from this setup. The acoustic emissions system bandpass filters the data from the piezo sensor, and returns a root mean squared (RMS) average amplitude to the data acquisition system. After applying the same 1000 point moving average filter to the

RMS signal, the resultant average amplitude shows excellent correlation to the force signal. The force data appears to have a lower threshold for detection of contact, however, afterwards, the two signal stay in phase, and are well-correlated.

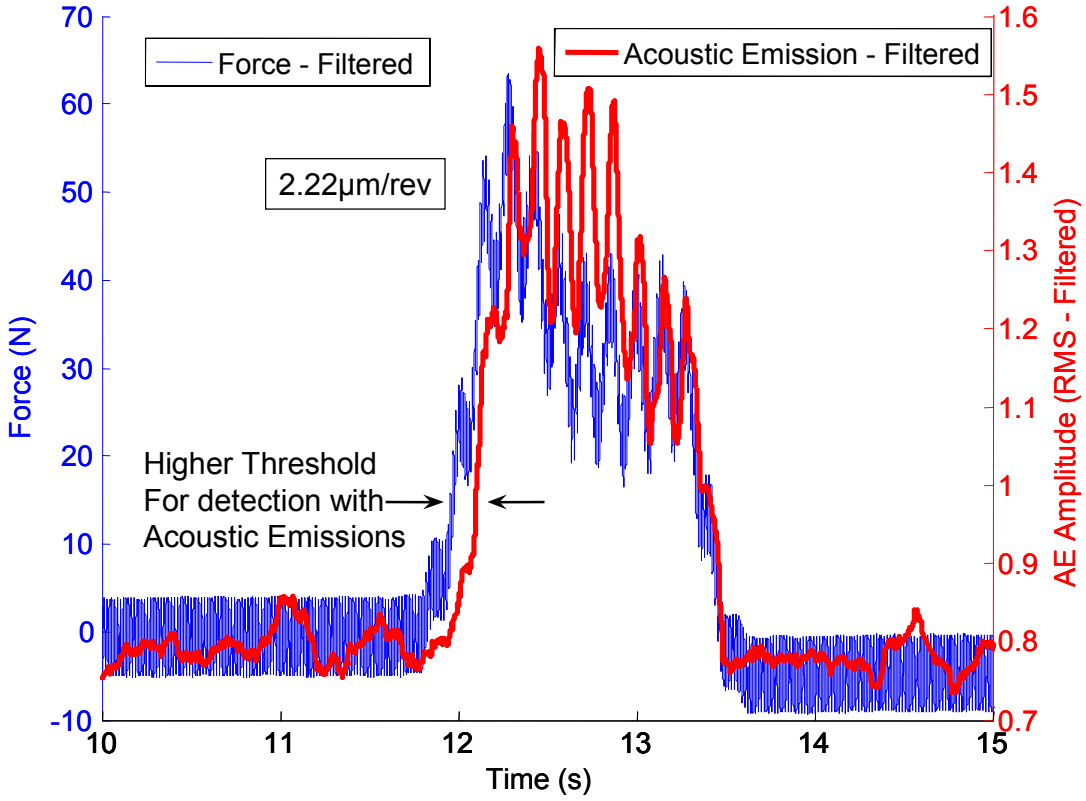

Figure 3.9: Force vs. Time and Acoustic Emissions RMS Amplitude vs. Time

4 Conclusions and Recommendations

4.1 Conclusions

- An experimental method to determine threshold forces in diamond roll plunge dressing has been developed.
- Experimental results suggest that two regimes exist, one below feed rates of approximately 3 mm/min exist and one above.

- Threshold forces normalized for grinding wheel width of 1.06 N/mm of wheel and 0.12 N/mm of wheel were experimentally determined for the feed rate regimes above and below 3mm/min, respectively.
- The Kaman Hall-effect sensors seem capable of measuring forces required to determine threshold forces when the experimental procedure described in this paper is followed.
- Neither the existence nor the values of the force threshold appear significantly affected by the filter parameters.

References

Hahn, Robert S.; "Influence of Threshold Forces on Size, Roundness and Contour Errors in Precision Grinding", Annals of the CIRP, v 30, n 1, Manufacturing Technology, General Assembly of CIRP, 31st, 1981, p 251-254.

Malkin, S.; "Grinding Technology Theory and Applications of Machining with Abrasives", Society of Manufacturing Engineers, ISBN 0-87263-480-9, 1989.

Proakis, J. P and Manolakis, D. G; "Digital Signal Processing Principles, Algorithms and Applications", III Ed., Prentice-Hall, 1996.

Robert S. Hahn and Richard P. Lindsay; "The Influence of Process Variables on Material Removal, Surface Integrity, Surface Finish and Vibration in Grinding"; Proceedings of the 10th international M.T.D.R. Conference, University of Manchester, September 1969; Pergamon Press, Oxford & New York 1970.

Richard P. Lindsay and Robert S. Hahn; "On the Basic Relationships between Grinding Parameters"; Annals of the CIRP, 19, 1971, p.657.

Robert I. King and Robert S. Hahn; "Handbook of Modern Grinding Technology", Chapman & Hall 1986.

Subramanian, K. and Keat, P. P.; "Parametric Study of Grindability of Structural and Electronic Ceramics – Part 1", American Society of Mechanical Engineers, Production Engineering Division (Publication) PED, v 17, 1985, p 25-32.

5 Appendix A: Nomenclature

Table 3: Nomenclature

D_{avg}	Average grinding wheel diameter	Mm
F_n	Normal Dress Force	N
F_n'	Normalized Normal Dress Force	N/mm width of grinding wheel
F_{th}	Threshold Force	N
F_{th}'	Normalized Threshold Force	N/mm width of grinding wheel
h	Grinding wheel wear	µm
Δh	Amount of over-dress	µm
K_{sys}	System stiffness	N/mm
K_{vf}	Voltage-force conversion factor	Volts/Newton
Q	Material Removal Rate	mm^3/min
Q'	Normalized Material Removal Rate	mm^3/min/mm width of grinding wheel
t	Time	Seconds
u_x	Crosshead feed rate	mm/minute
V	Voltage	Volts